Synthesis and characterization of two- and three-dimensional calcium coordination polymers built with benzene-1,3,5-tricarboxylate and/or pyrazine-2-carboxylate

Raj Kishore Vakit†i, Brady D. Garabato†, Natalie P. Schieber†, Melinda J. Rucks‡, Yan Cao†, Cathleen Webb†, Jeremy B. Maddox†, Aaron Celestian, Wei-Ping Pan†, Bangbo Yan†**

Department of Chemistry†, Geography and Geology†, Western Kentucky University, 1906 College Height Blvd, Bowling Green, KY 42101, USA

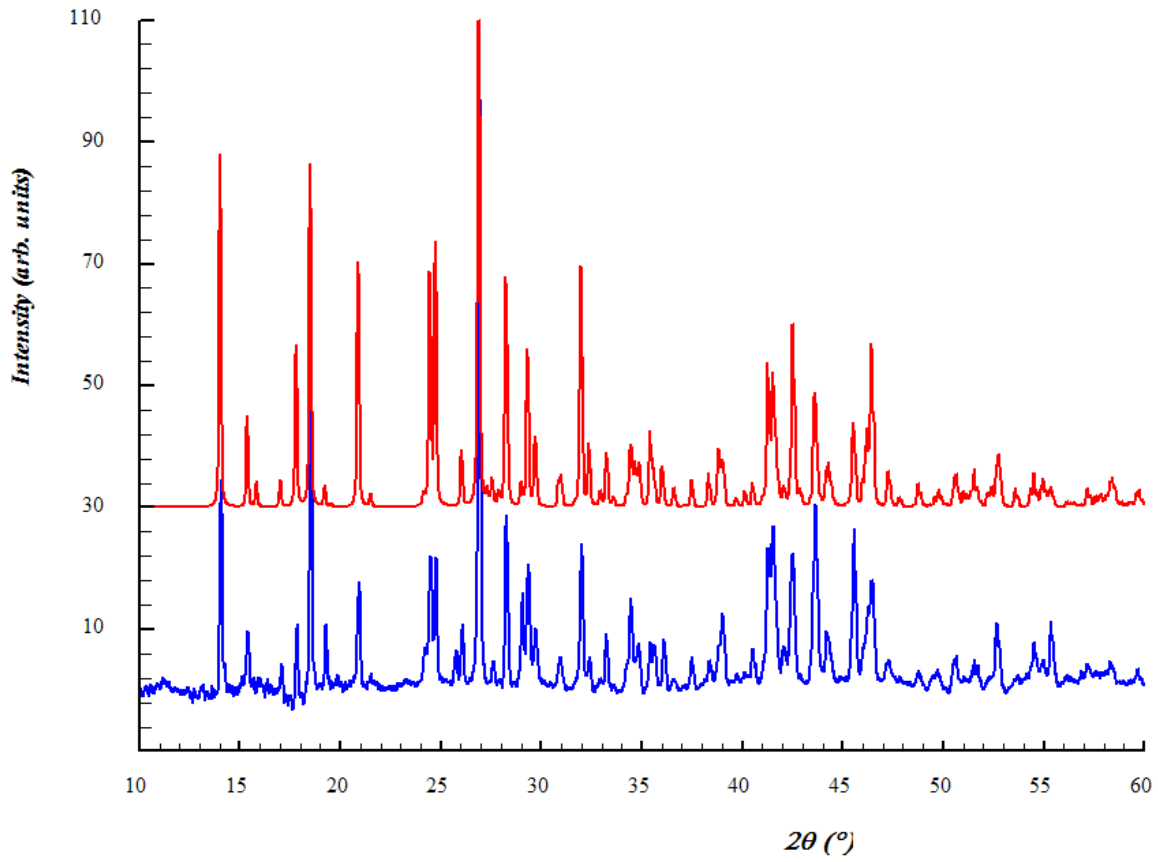

Figure s1. Experimental (blue) and simulated (red) powder X-Ray patterns of compound **1**.

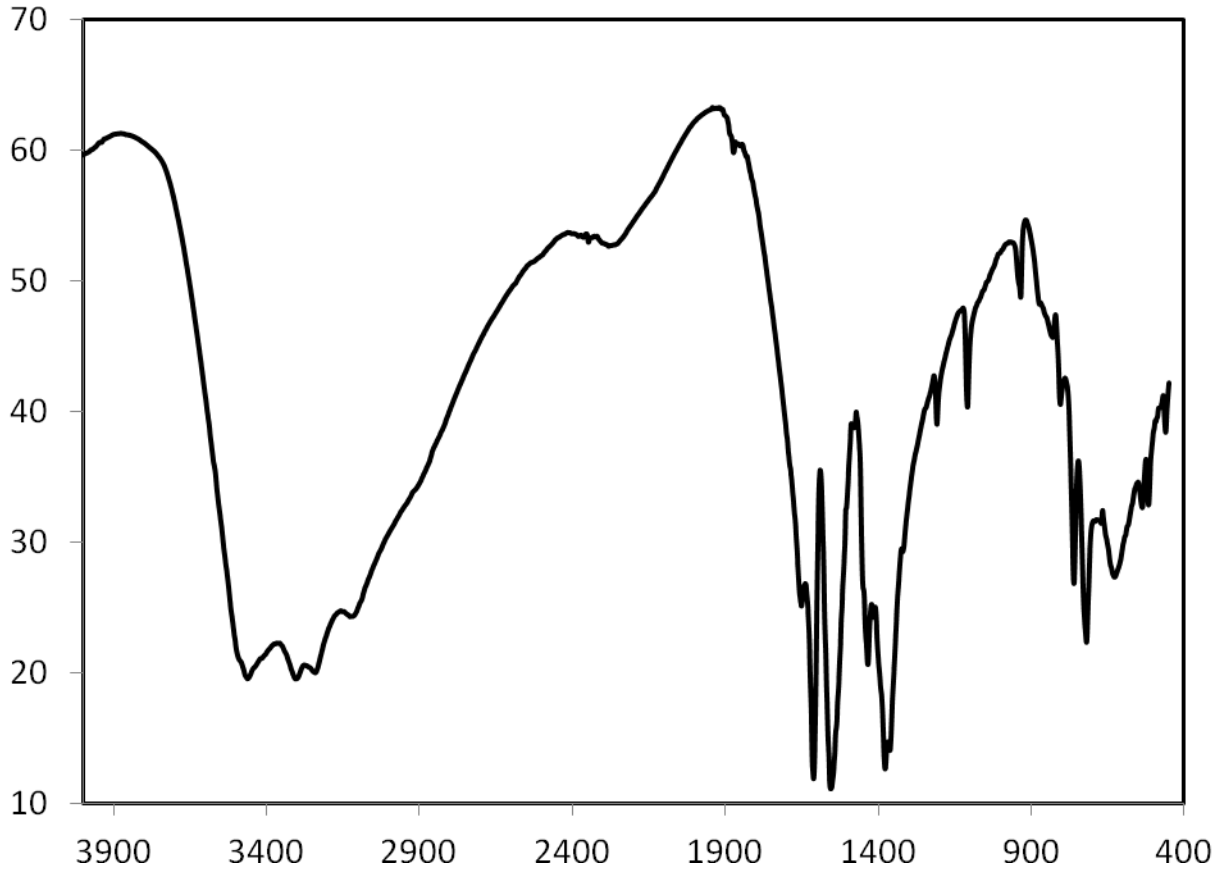

Figure s2. IR spectra of compound **1** (KBr).

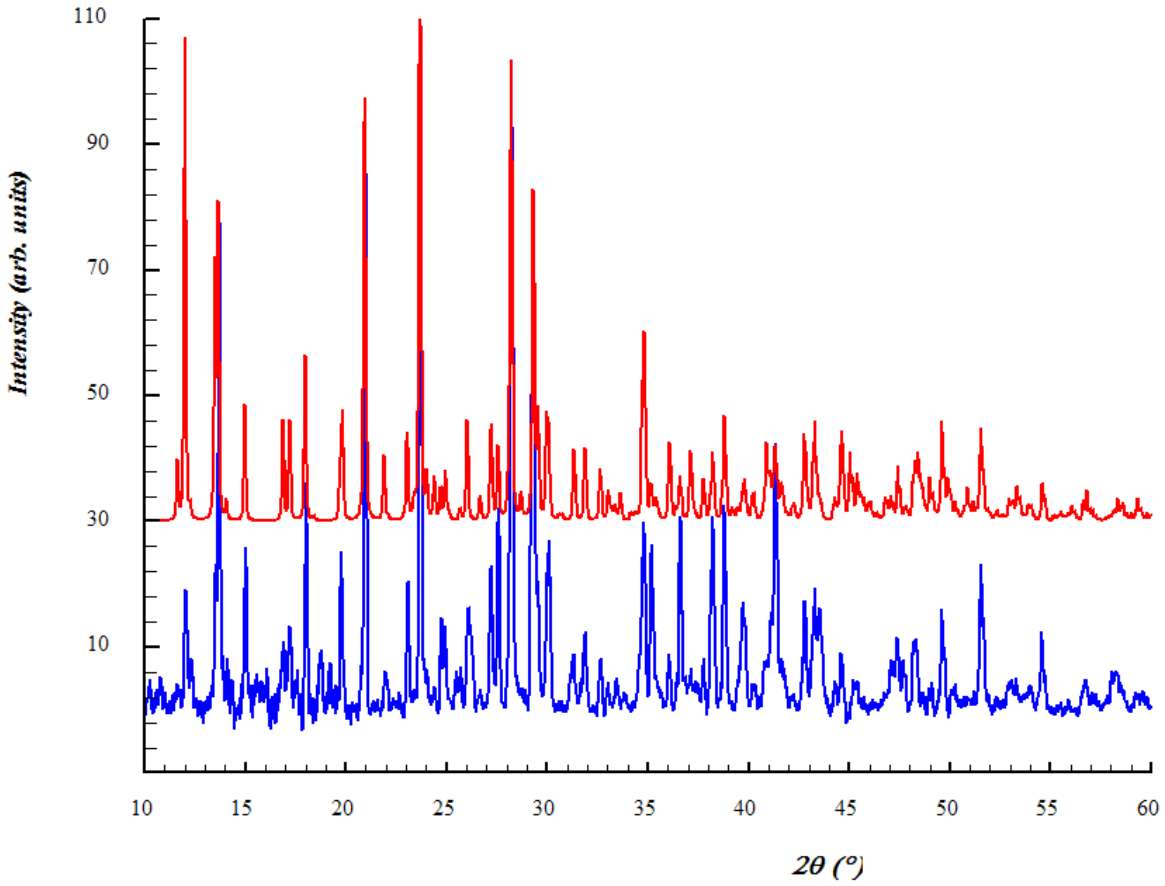

Figure s3. Experimental (blue) and simulated (red) powder X-Ray patterns of compound **2**.

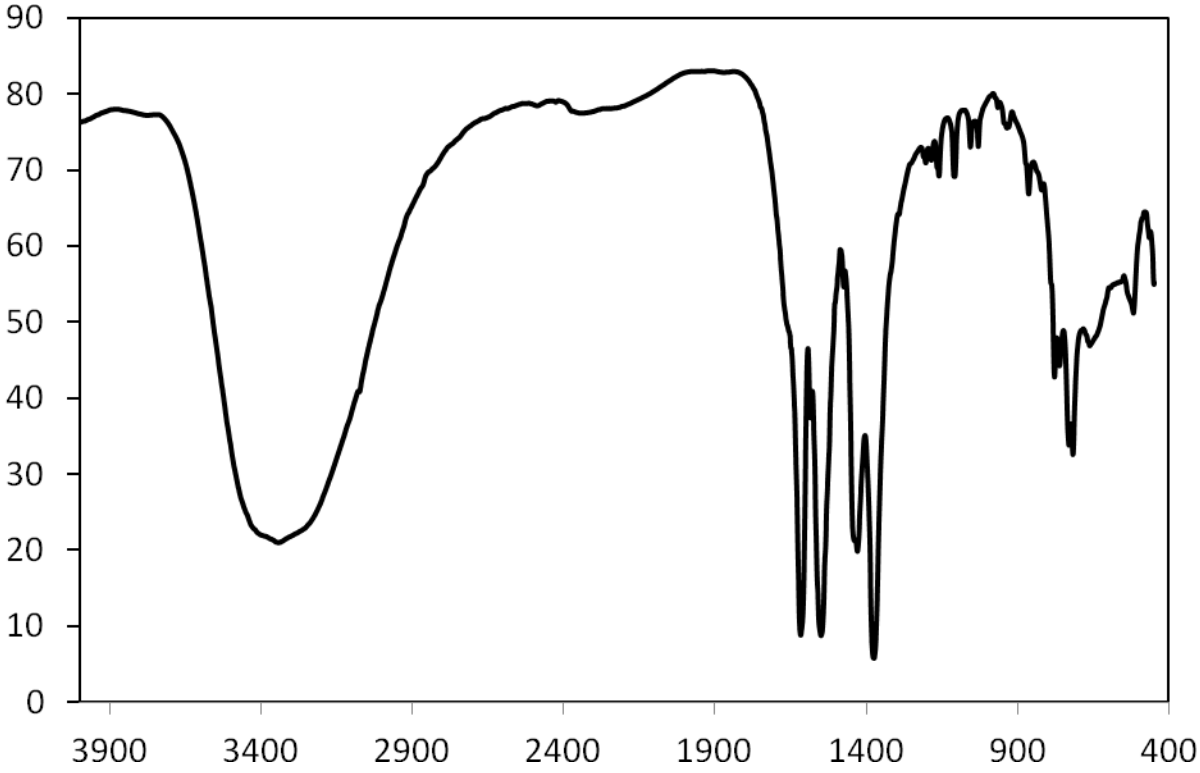

Figure s4. IR spectra of compound **2** (KBr).

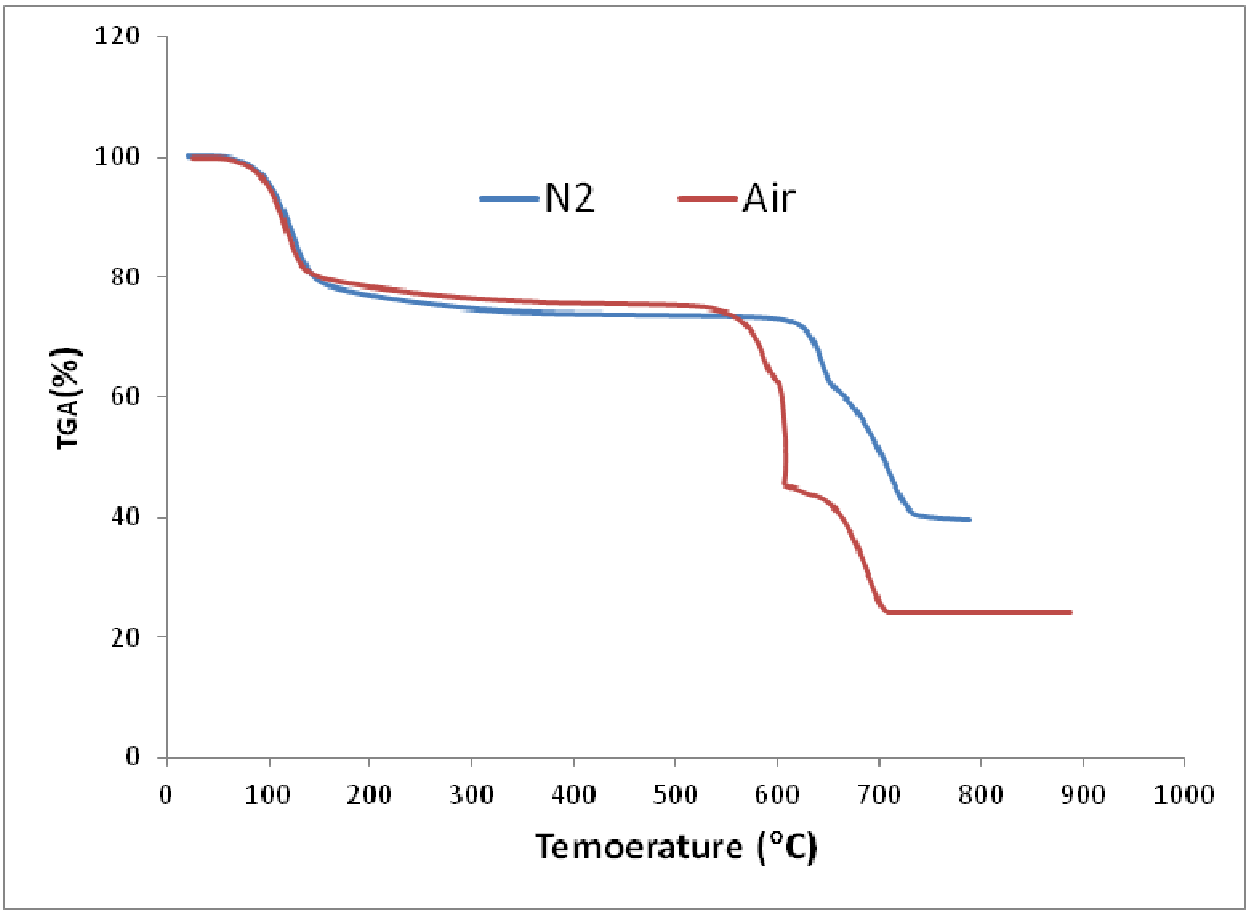

Figure s5. TGA plots of compound **1** in air and nitrogen

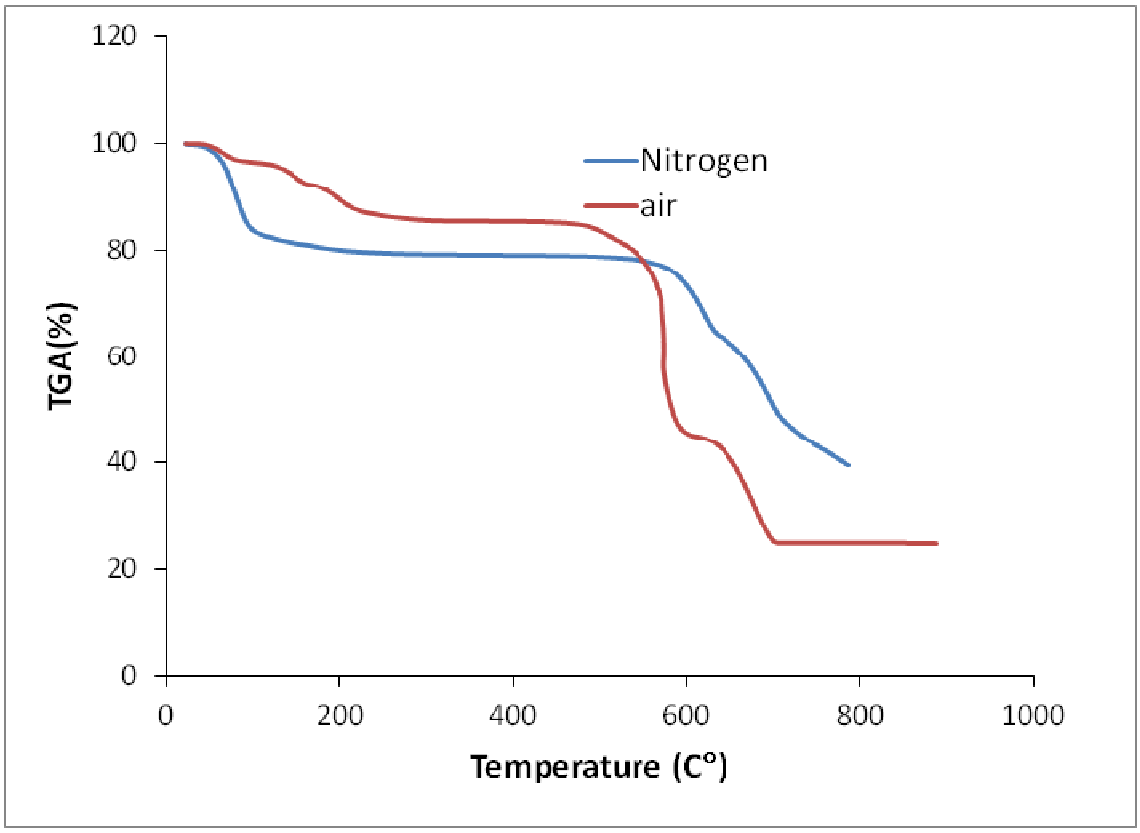

Figure s6. TGA plot of compound **2** in air and nitrogen

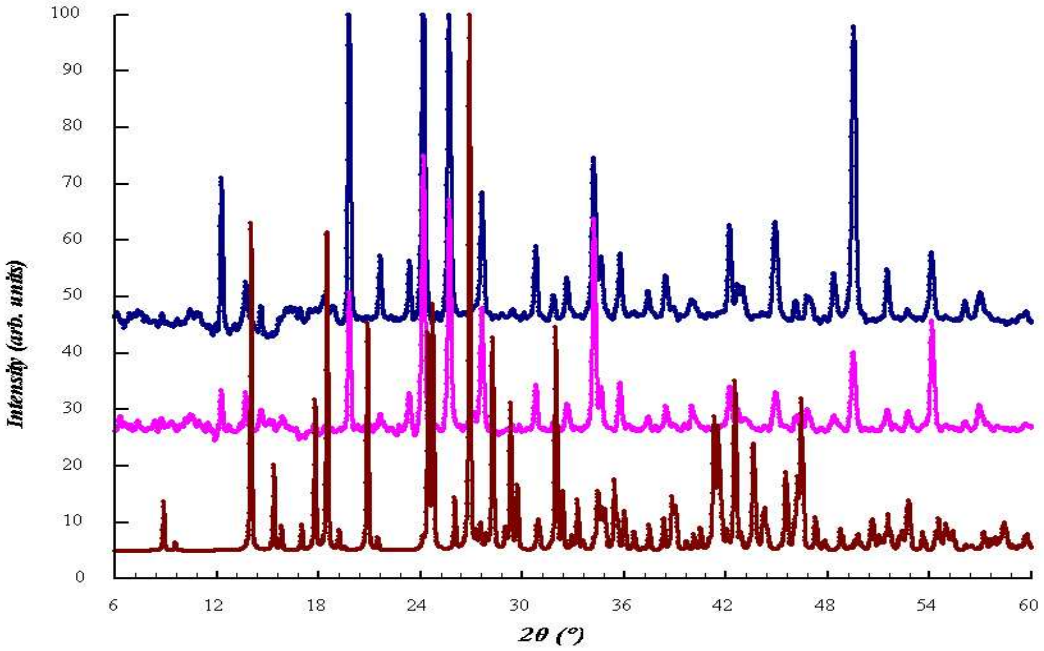

Figure s7. PXRD pattern of **1**: simulated (brown), after heated at 150 °C (pink), at 200°C (blue)

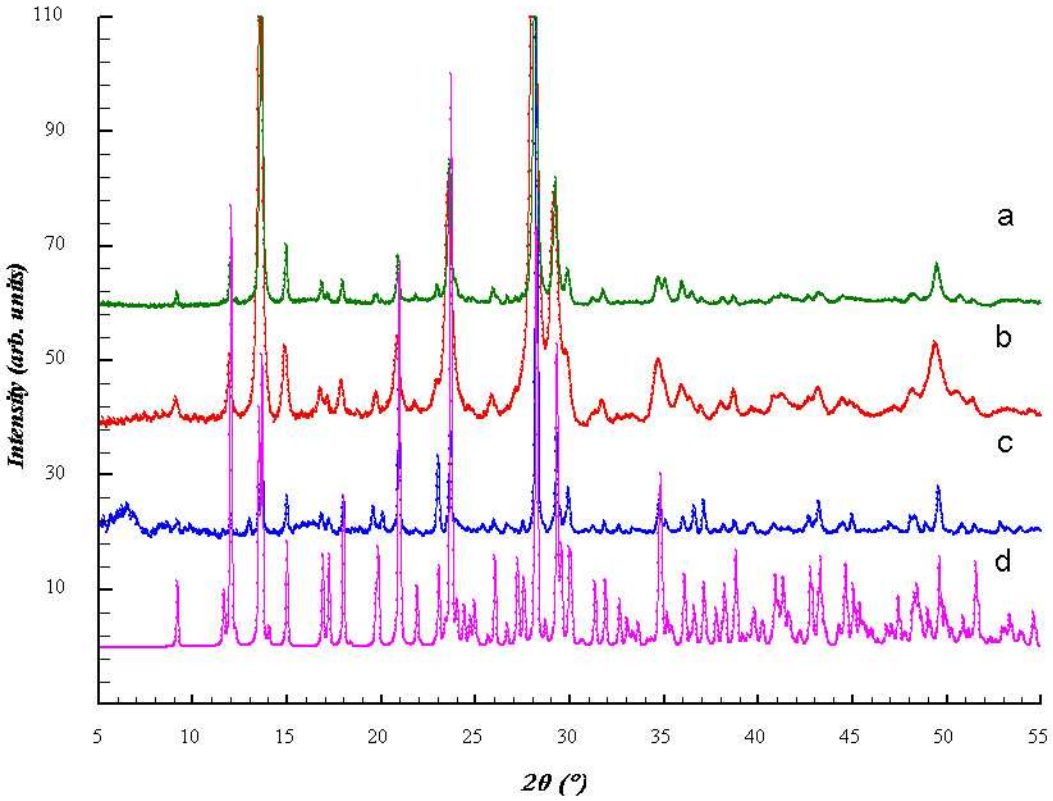

Figure **s8**. PXRD pattern of **2**: heated at (a) 250°C, (b) 200 °C , (c) 150°C in air for 12 hours; and simulated from single crystal structure (d).

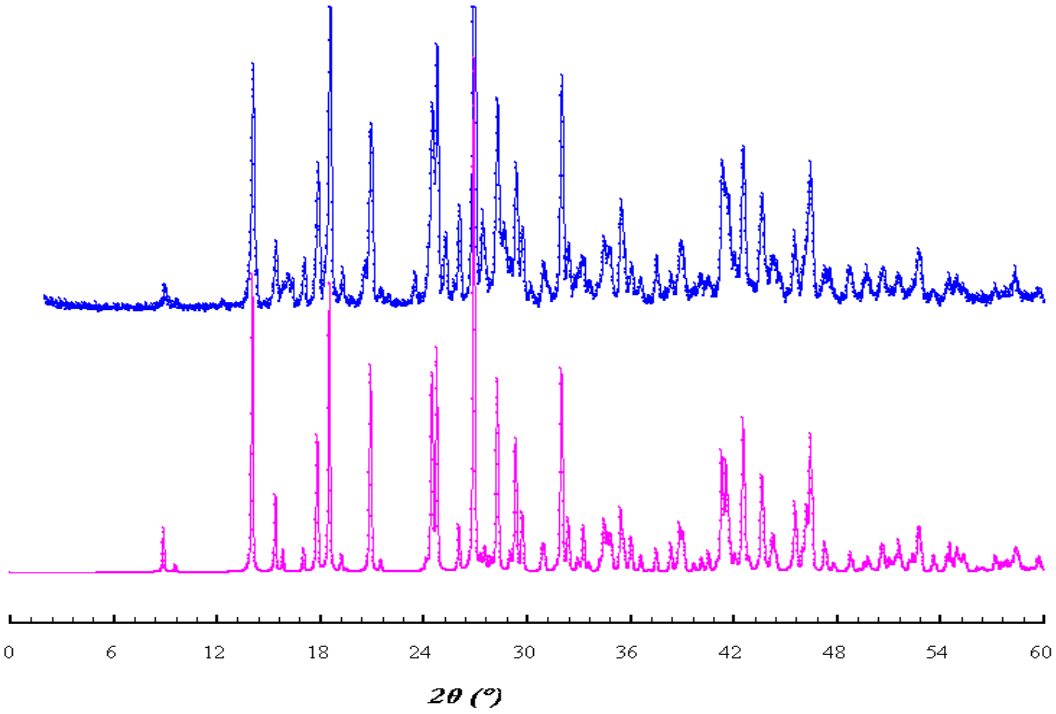

Figure s9. PXRD of simulated and rehydrated form of compound **1** at 200°C

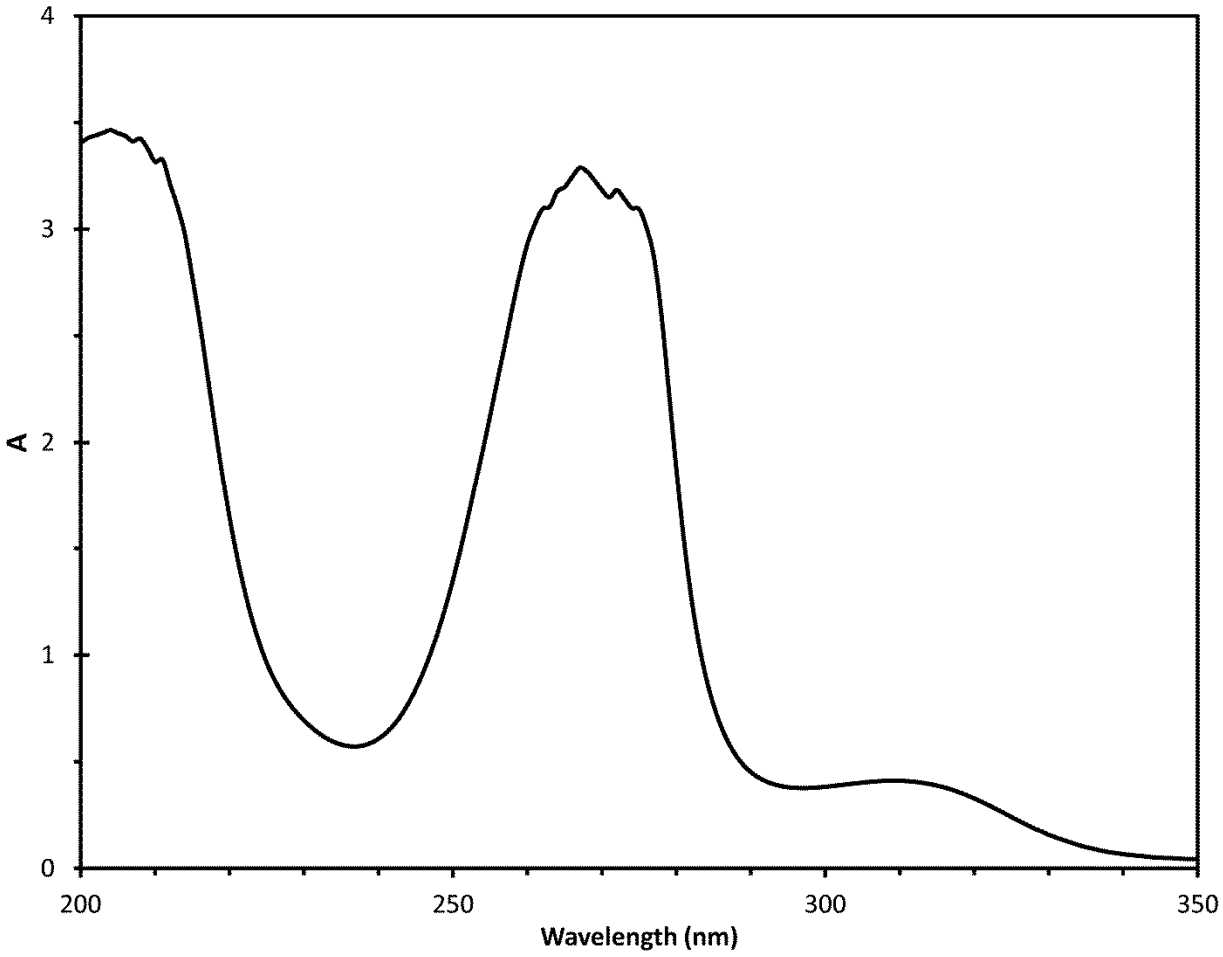

Figure s10. UV-vis spectra of free Hpzc ligand in aqueous solution

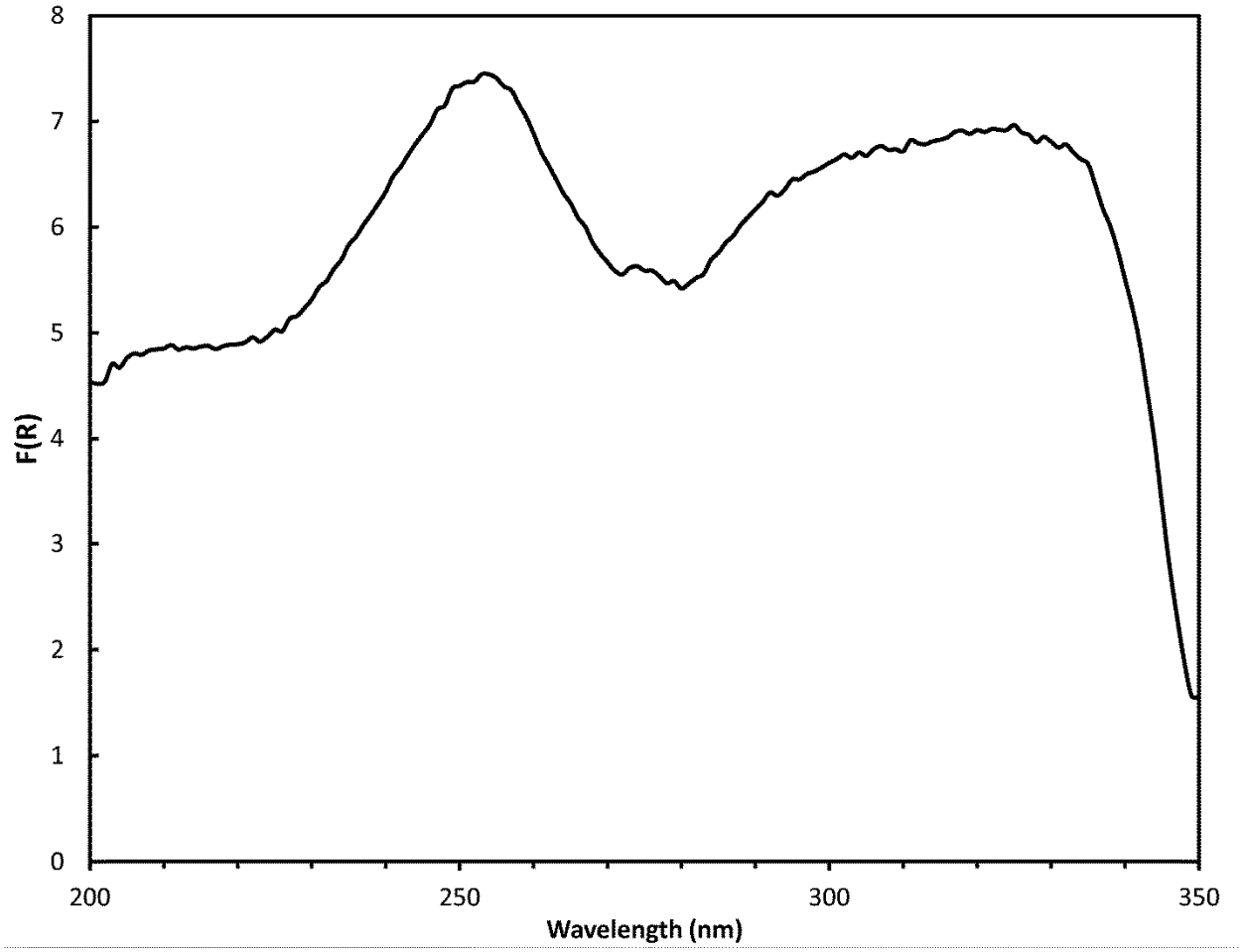

Figure s11. UV-vis Diffuse reflectance spectra of Hpzc

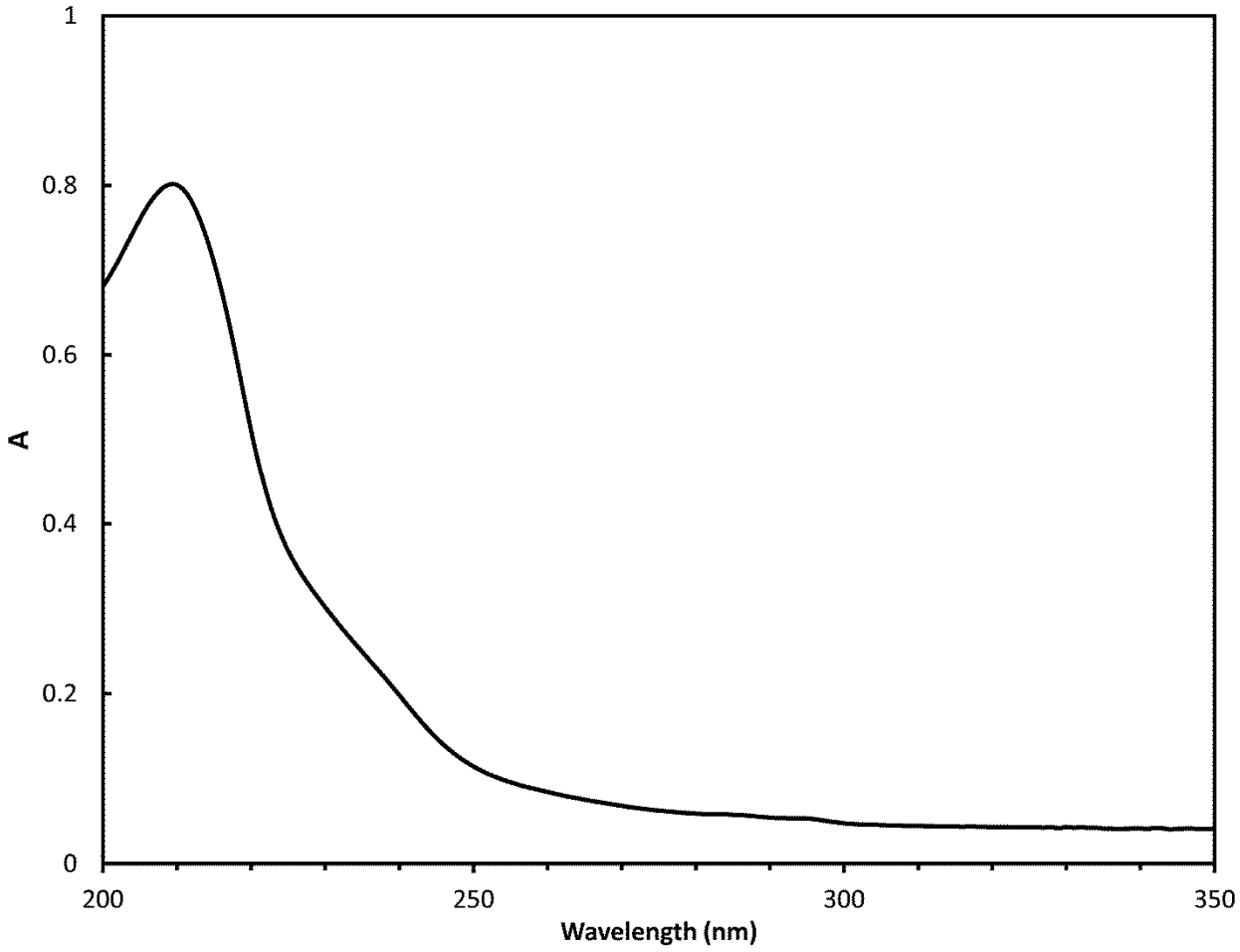

Figure s12. UV-vis spectra of H_3btc in aqueous solution

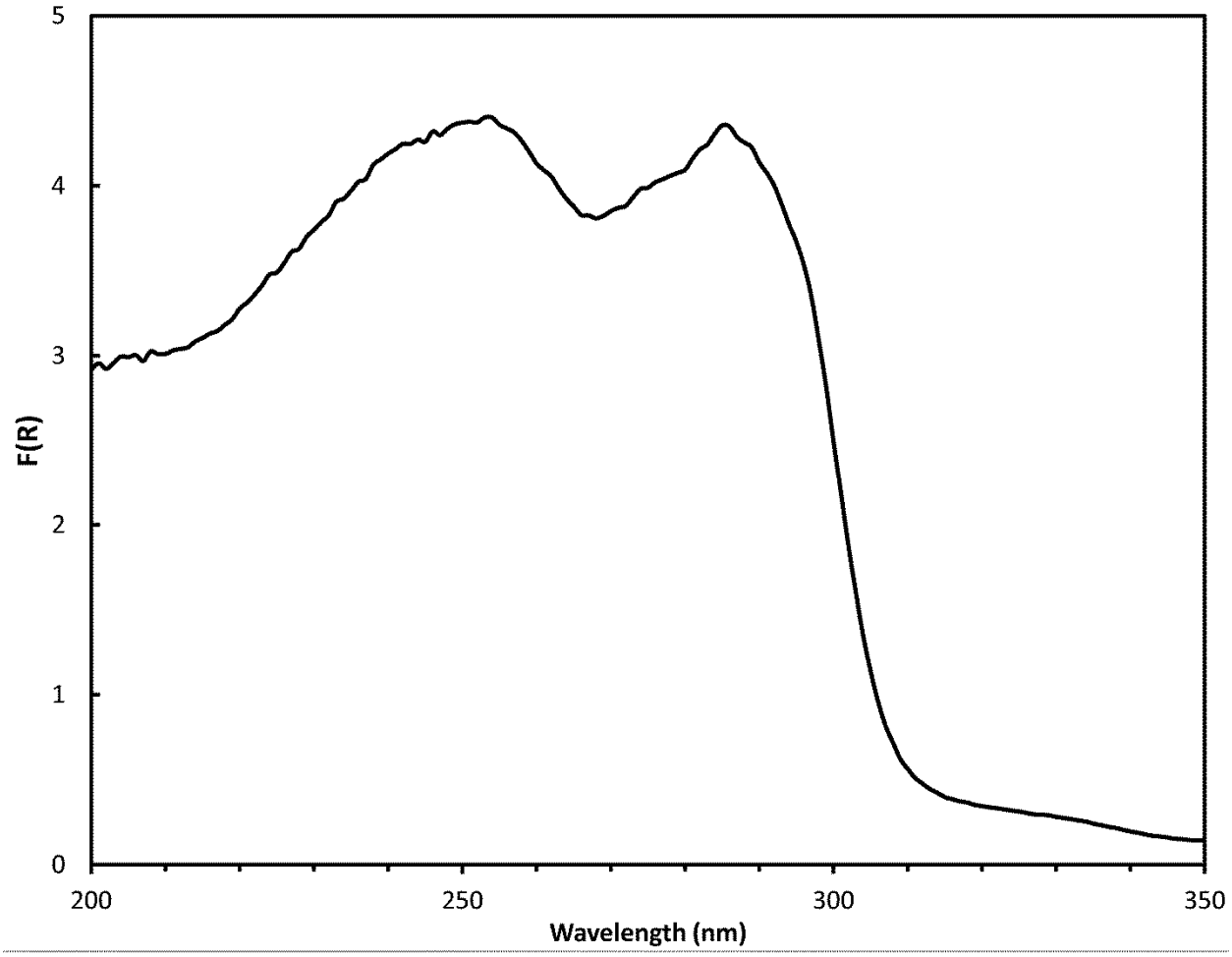

Figure s13. UV-vis Diffuse reflectance spectra of H_3btc

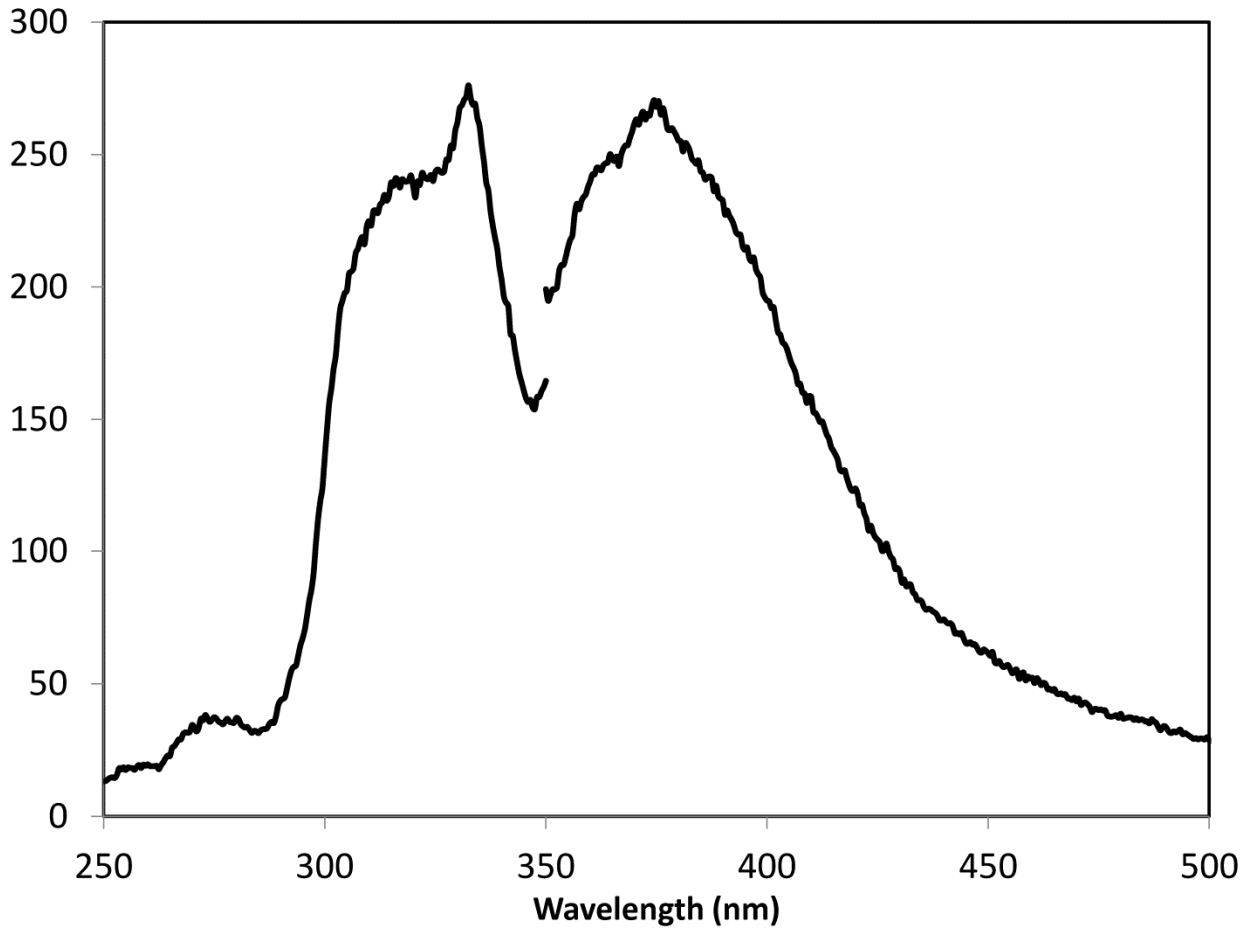

Figure s14. The emission and excitation spectra of free ligand H_3btc

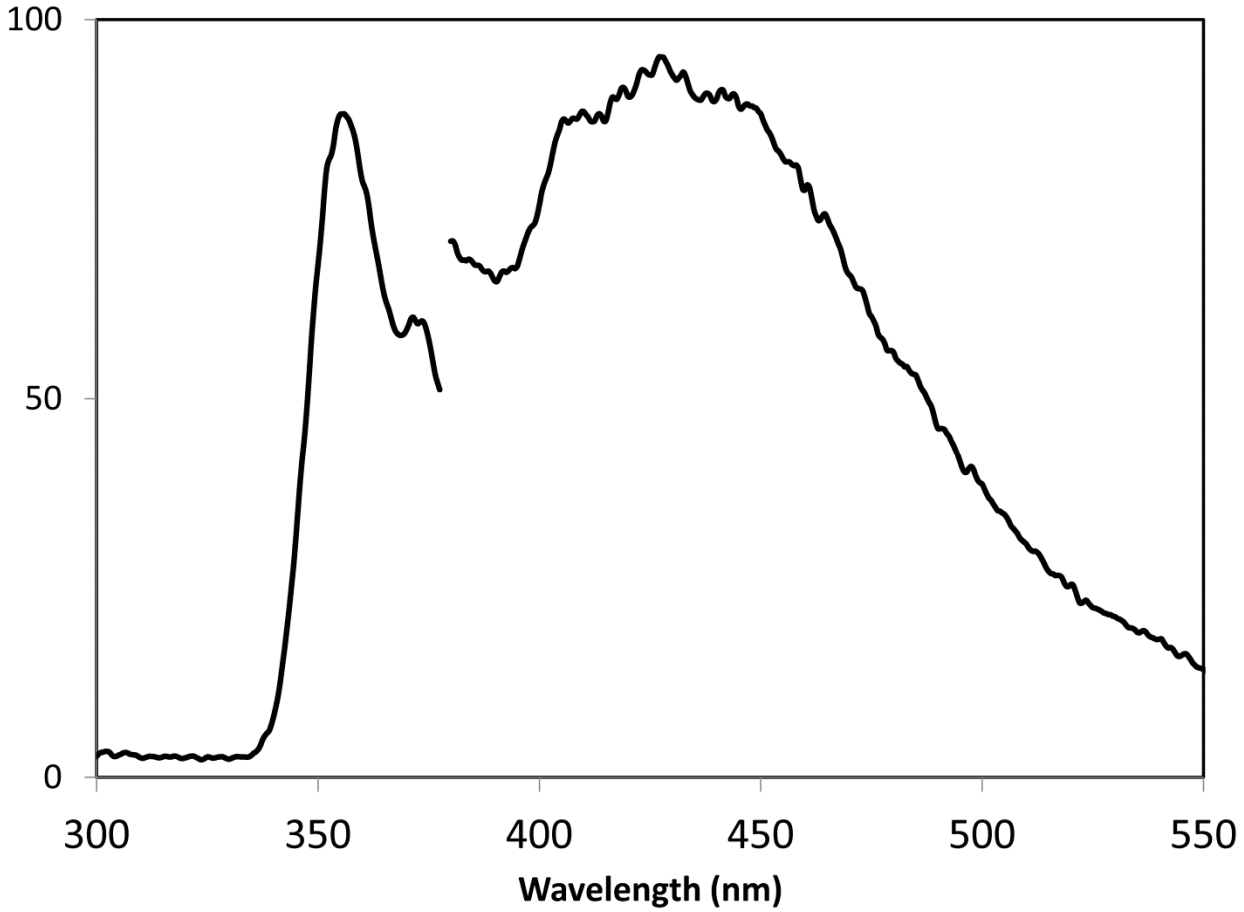

Figure s15. The emission and excitation spectra of free ligand Hpzc

Table S1. Selected Bond Lengths [Å] for compounds **1** and **2**.

Compound 1		Compound 2	
Ca(1)-O(2)#1	2.299(1)	Ca(1)-O(4)#1	2.297(1)
Ca(1)-O(4W)	2.330(1)	Ca(1)-O(6)#2	2.411(1)
Ca(1)-O(5)#2	2.342(1)	Ca(1)-O(7)#2	2.413(1)
Ca(1)-O(1W)	2.398(1)	Ca(1)-O(2)	2.462(1)
Ca(1)-O(3W)	2.436(1)	Ca(1)-O(1W)	2.478(2)
Ca(1)-O(2W)	2.454(1)	Ca(1)-O(2W)	2.518(2)
Ca(1)-O(5W)	2.967(2)	Ca(1)-O(1)	2.586(1)
		Ca(1)-O(8)#2	2.771(2)
Ca(2)-O(6W)#3	2.335(2)	Ca(2)-O(3)#3	2.300(1)
Ca(2)-O(6W)	2.335(2)	Ca(2)-O(1)	2.322(1)
Ca(2)-O(4)#3	2.490(1)	Ca(2)-O(3W)	2.366(2)
Ca(2)-O(4)	2.490(1)	Ca(2)-O(7)	2.394(1)
Ca(2)-O(5W)#3	2.539(2)	Ca(2)-O(5)#2	2.396(2)
Ca(2)-O(5W)	2.539(2)	Ca(2)-O(6)#2	2.552(2)
Ca(2)-O(3)	2.543(1)	Ca(2)-N(1)	2.596(2)
#1 -x+2,-y+2,-z; #2 -x+3/2,-y+3/2,-z; #3 -x+2,y,-z+1/2		#1 -x+3/2,-y,z-1/2; #2 -x+1/2,-y,z-1/2; #3 x-1,y,z	

Electronic Structure Calculations and Optical Spectra

Free acids (H_3btc and Hpzc) and ions (btc and pzc) in water

Quantum chemistry geometry optimizations were performed to obtain gas phase minima energy structures of the free H_3btc and Hpzc acis and the btc (-3) and pzc (-1) anions. These calculations were carried out using the PBEPBE/cc-pVDZ model chemistry and a normal modes frequency analysis was used to confirm that the final structures were local minima. A second set of geometry optimizations and frequency calculations were carried out for all species using a self-consistent reaction field (SCRF) to model the effects of an implicit water solvent. Finally, the electronic transitions of the solvated species were calculated using the TD-DFT method and the dominant transitions were examined using an NTO analysis. The results of these calculations can be compared with the experimental UV spectrum of H3btc and Hpzc in aqueous solution.

H_3btc in water

The simulated spectrum for H3btc in water is shown below in **Figure s16** and consists of four dominant lines at 253, 242, 229, and 217 nm. Each line is comprised of a pair of nearly degenerate electronic transitions, and these correspond very well with the experimental UV spectrum of H3btc in water, which shows a band at 209 nm and a shoulder at 238 nm. Lower energy transitions in the 280-350 nm range of the simulated spectrum have negligible or vanishing oscillator strengths, and we cannot identify the very weak experimental band at 294 nm from this calculation.

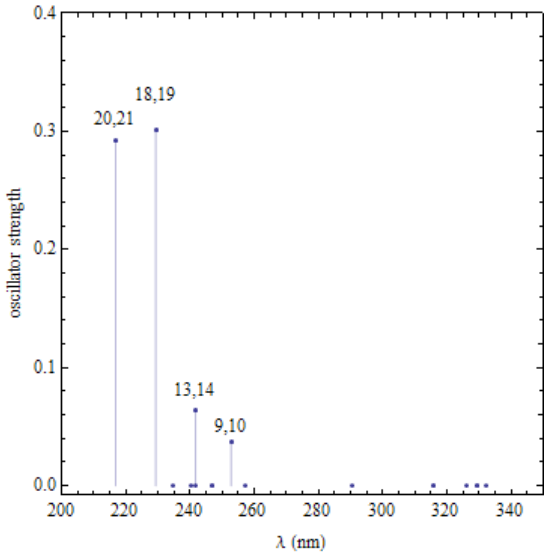

Figure s16. Calculated UV spectra of H_3btc in water.

The lowest energy line at 253 nm is due to transitions from the ground state to excited states 9 and 10. The most significant NTO hole/particle pairs for these transitions are shown in **Figure s17**. For both transitions, the NTO pairs are enumerated (1 and 2 in this case) and are further

labeled as either h or p to identify the orbital as either a hole or particle, respectively. For both states 9 and 10, the first NTO pair represents 28% of the electronic transition, while the second pair is the more dominate contribution with a weight of 72%. For all NTO pairs, the holes contain a significant contribution from the carbon-oxygen π bond of various carbonyl groups, which is strongly polarized towards the oxygen atom because of its greater electronegativity. It is interesting to note, however, that there is also a significant contribution coming from the p-type lone pair on the hydroxyl oxygen atom. The corresponding particles all clearly exhibit a π* anti-bonding pattern within the phenyl ring. Despite the fact that the contribution from the hydroxyl groups is technically non-bonding, it is most sensible to identify the transitions for this spectral line as π → π* type and involving charge transfer from the carboxylic acid groups to the phenyl ring.

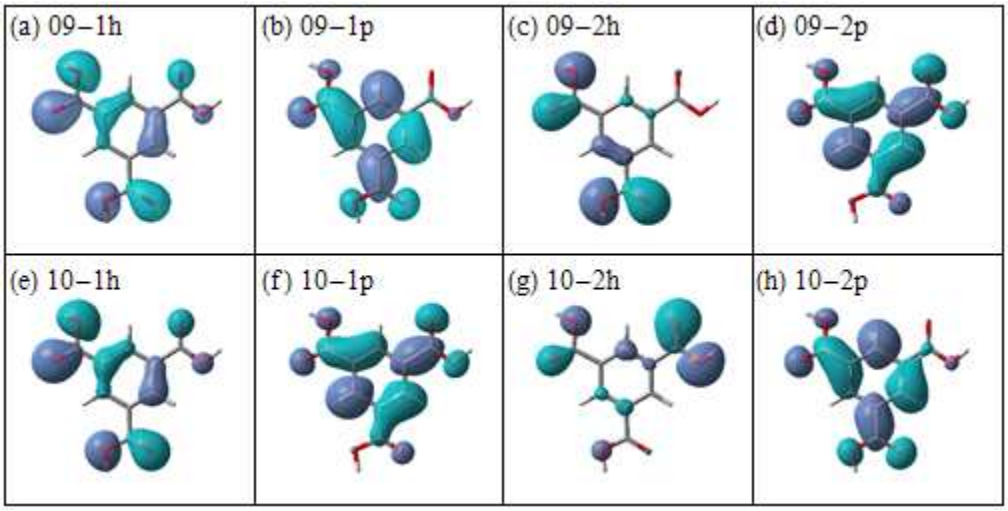

Figure s17. NTO hole/particle pairs for the calculated electronic transitions of H3btc at 253 nm.

The next line at 242 nm is due to transitions to states 13 and 14. The NTO hole/particle pairs for these transitions are shown in **Figure s18**. Like the previous line, there are two dominant NTO pairs for these transitions. The contributions made by NTO pairs 1 and 2 are 27% and 68%, respectively, for state 13 and 29% and 66%, respectively, for state 14. The 5% difference (from 100%) for both transitions is comprised of NTO pairs with much smaller weights. Like before, we see that the NTO holes seem to consist of both n-type character on the hydroxyl oxygen atoms and π bonding within carbonyl groups; however, there is also some contribution from carbon-carbon π bonds within the phenyl ring. The NTO particles are π* anti-bonding within the phenyl ring and to some extent on certain oxygen atoms. We classify these transitions as π→ π* type transitions.

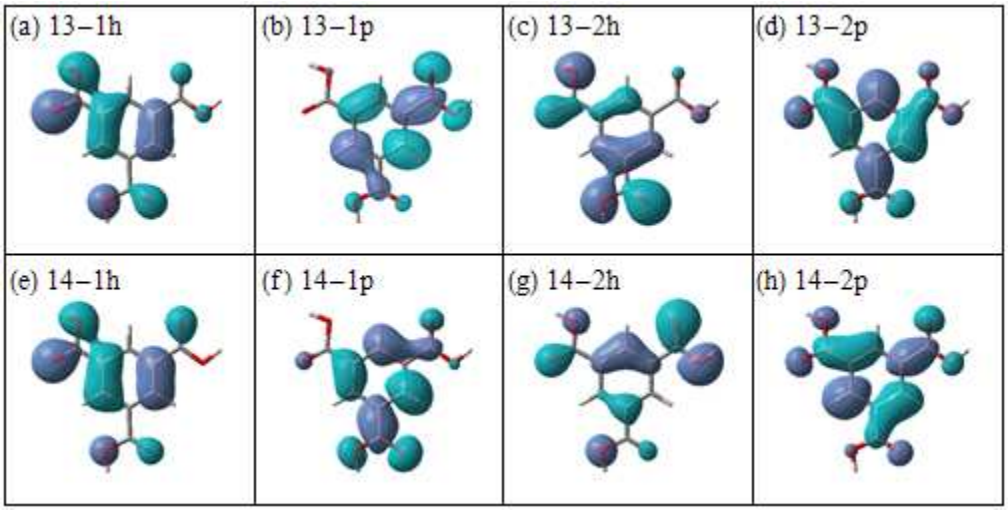

Figure s18. NTO hole/particle pairs for the calculated electronic transitions of H3btc at 242 nm.

The most dominant spectral line at 229 nm is due to transitions to states 18 and 19. The NTO hole/particle pairs for these transitions are shown in **Figure** s19. Again, there are two dominant NTO pairs for each transition; however, the weights are more or less equal: 45% and 47% for state 18 and 44% and 49% for 19. For both transitions, the NTO holes exhibit a very clear π bonding pattern within the phenyl ring and the NTO particles have π* anti-bonding character. We classify these as π→ π* transitions.

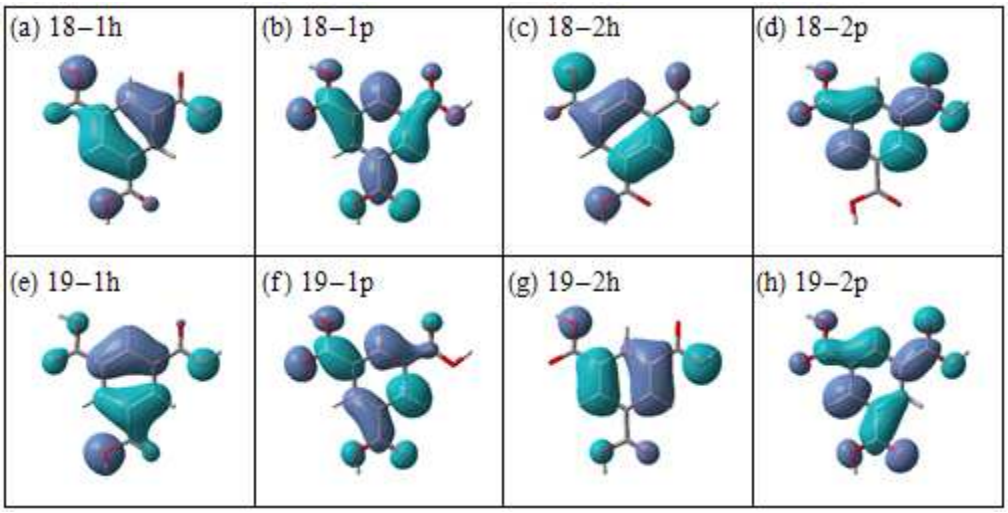

Figure s19. NTO hole/particle pairs for the calculated electronic transitions of H_3btc at 229 nm.

The higher energy line at 217 nm is due to transition to states 20 and 21, and the NTO hole/particle pairs are shown **Figure s20**. There is only dominant pair for state 20, with a weight of 87%, such that other NTO pairs all have weights less than 10%. For state 21, there are two NTO pairs with weights greater than 10%. The first NTO pair represents 11% of the transition, and the second pair contributes 87%. For both state 20 and 21, the dominant NTO pairs are consistent with $\pi \rightarrow \pi^*$ transitions; however, there are clearly more nodes in the NTO particle, which would correspond to a higher energy π^* orbital.

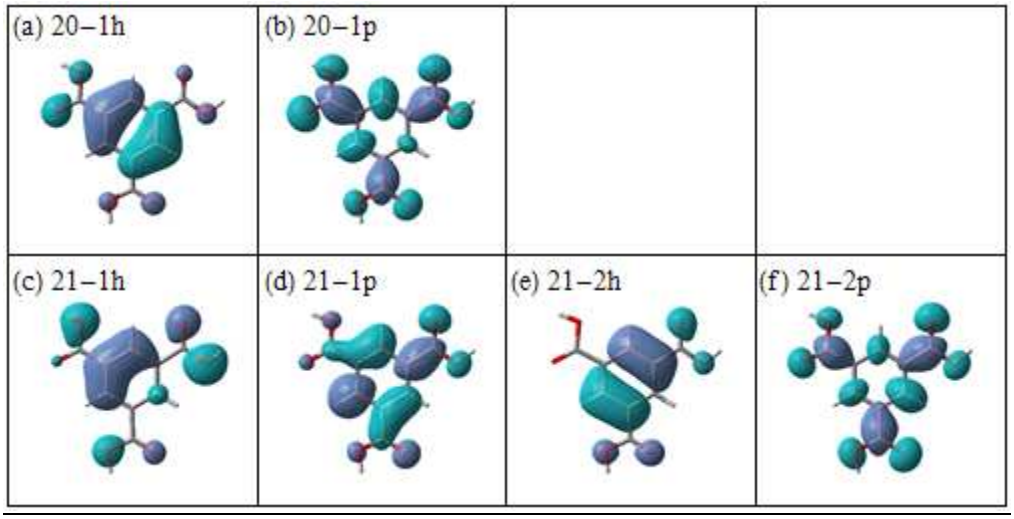

Figure s20. NTO hole/particle pairs for the calculated electronic transitions of H3btc at 217 nm.

btc ion in water

The simulated electronic spectrum for the btc ion in water is shown **Figure s21**. There are three dominant lines with non-negligible oscillator strengths at 323, 221, and 208 nm. Because of the ion's symmetry, these lines are again due to doubly degenerate electronic transitions.

The 323 nm line at low energy could possibly correspond to the observed very weak band in the experimental spectrum at 294 nm, although the calculated transition is significantly lower in energy. Nevertheless, this seems to be only transition for H3btc or btc with significant oscillator strength and a wavelength greater than 280 nm.

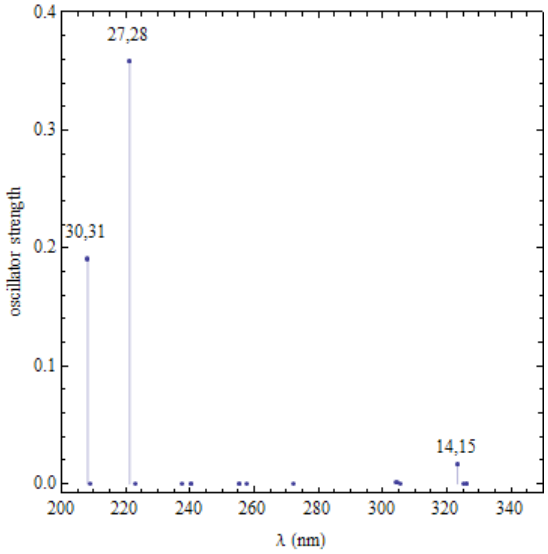

Figure s21. Calculated UV spectrum of btc ion in water.

The calculated 323 nm line is due to transitions to states 14 and 15. The NTO hole/particle pairs for these transitions are shown in **Figure s22**. There are two dominant NTO pairs for each transition. The weights for pairs 1 and 2 corresponding to state 14 are 24% and 76%, respectively. The weights for state 15 are 21% and 79% for NTO pairs 1 and 2, respectively. The NTO holes appear to resemble p-type lone pairs orbitals on the oxygen atoms. However, closer inspection shows that for each hole the phase on adjacent oxygen atoms are opposite of one another. This is likely to due to the anti-symmetric combination of two neighboring carbon-oxygen π-type bonds, such there is a node on the bridging carbon atom. The corresponding particles have a π* anti-bonding pattern within the phenyl ring. We identify these transitions as π→ π* type.

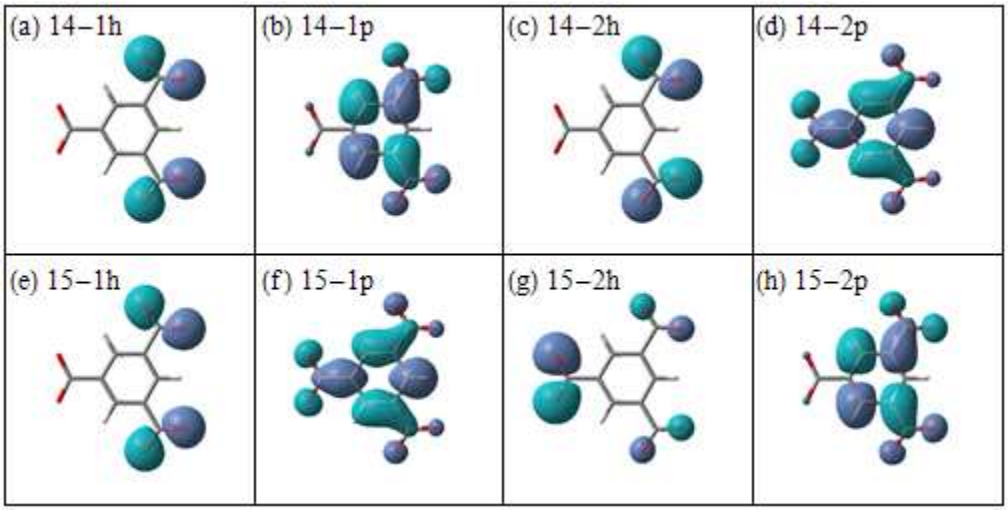

Figure s22. NTO hole/particle pairs for the electronic transitions of btc ion at 323 nm.

The dominant spectral line at 221 nm is due to transitions to 27 and 28. The two NTO hole/particle pairs for both of these transitions are shown in **Figure s23**. The weights are 45%-45% for pairs 1 and 2, respectively, for both states 27 and 28. The NTO holes have a π bonding character and the NTO particles are π*, and so we identify these as π→ π* type transitions.

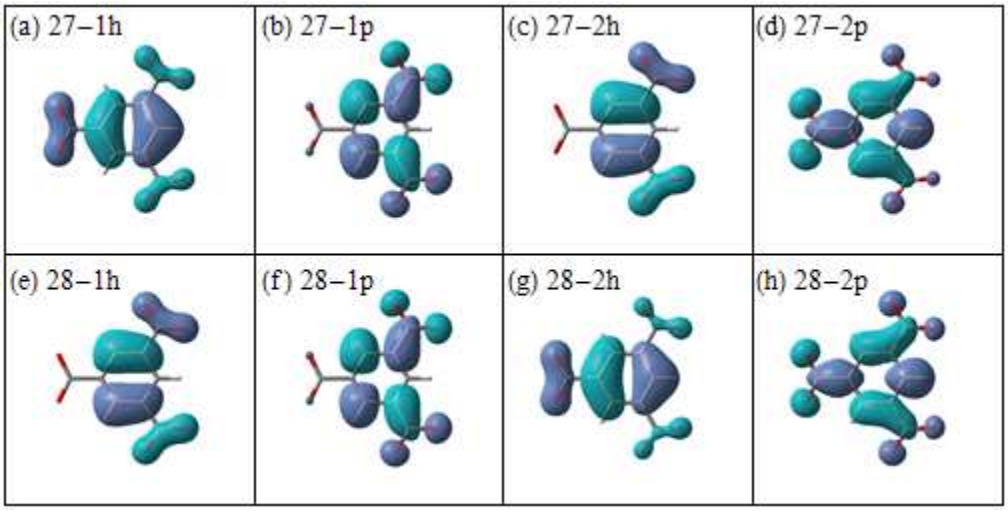

Figure s23. NTO hole/particle pairs for the electronic transitions of btc ion at 221 nm.

The high energy line at 208 nm is due to transitions to states 30 and 31, and there is only one dominant NTO hole/particle pair with a weight of 83% for each state. The NTO pairs are shown in **Figure s24**, where we see that the NTO holes for both states are similar to the anti-symmetric combination of carbon-oxygen π bonds within the carbonyl groups, and the corresponding particles are high energy π* anti-bonding orbitals with many nodes. We classify this line as a π→ π* transition.

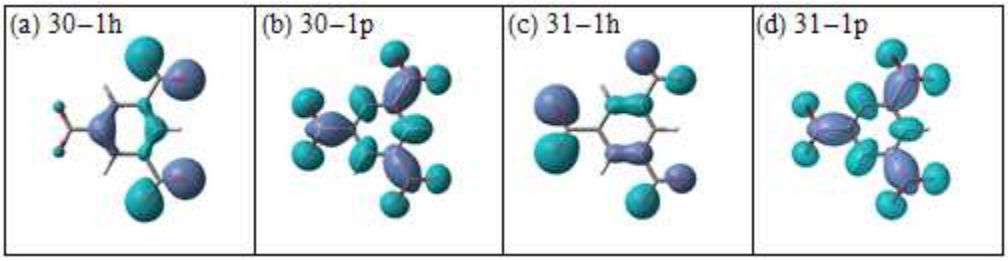

Figure s24. NTO hole/particle pairs for the electronic transitions of btc ion at 208 nm.

Hpzc in water

The simulated spectrum for Hpzc in water is shown in **Figure s25**. There are two dominant spectral lines at 254 and 219 nm. We associate these transitions with the observed bands at 268 nm and 205 nm in the experimental UV spectrum of Hpzc in water. From this calculation we are not able to identify an electronic transition corresponding to the observed band at 312 nm.

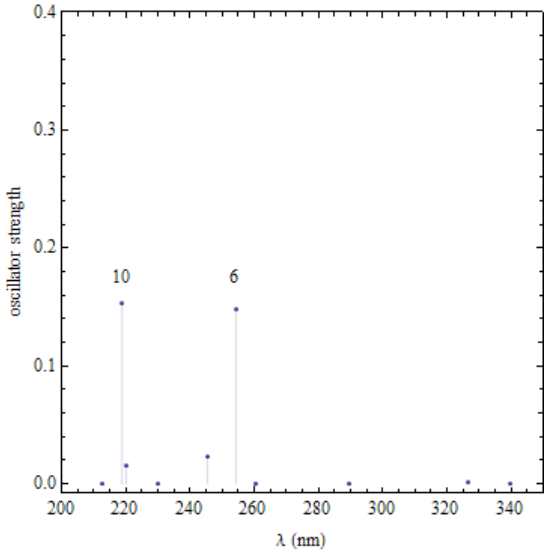

Figure s25. Calculated UV spectrum Hpzc in water.

The line at 254 nm is due to an electronic transition to state 6, and the line at 219 nm is due to a transition to state 10. There are two dominant NTO hole/particle pairs for each of these transitions, and these are shown in **Figure s26**. For the low energy transition, the first NTO pair represents 12% of the transition and the second pair has a weight of 88%. The two pairs for the higher energy transition have weights of 10% and 88%. In both transitions, the hole for the dominant NTO pair shows a strong π bonding character; however, there is also a non-negligible π bonding contribution from the carbonyl group. The corresponding NTO particles are clearly π* anti-bonding, and so we classify both of these transitions as π → π* type transitions.

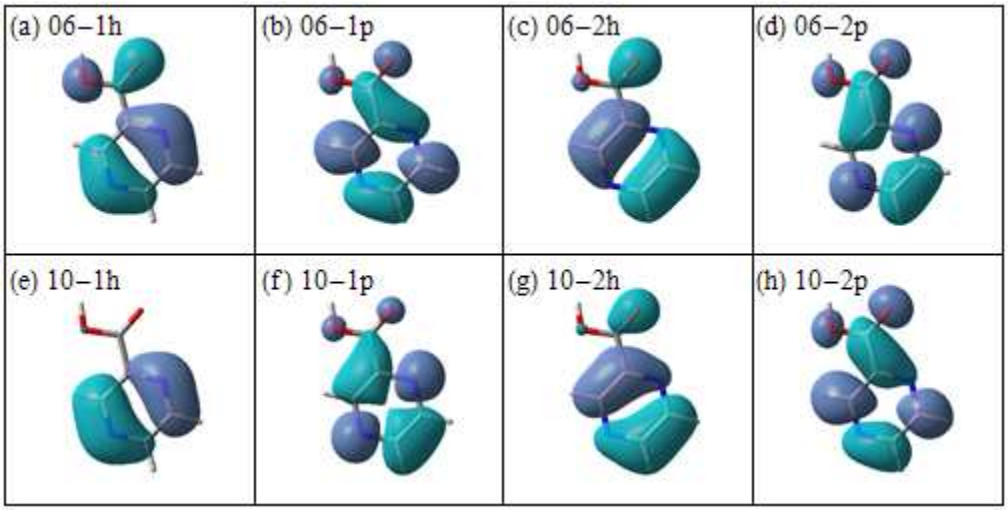

Figure s26. NTO hole/particle pairs for the electronic transitions of Hpzc at 254 and 219 nm.

pzc ion in water

The simulated spectrum for the pzc ion in water is shown in **Figure s27**, and is not significantly different from the acid. There are two dominant lines at 252 and 213 nm, which are due to transitions to states 9 and 14, respectively. Unfortunately, no low energy transitions with significant oscillator strength were obtained in this calculation, and so we cannot identify the weak absorption band at 312 nm in the experimental UV spectrum of Hpzc. Both states 9 and 14 have only one dominant NTO hole/particle pair, and these are shown in **Figure s28**. The NTO pair for state 9 has a weight of 90% and the weight of the NTO pair for state 14 is 89%. Both transitions can be identified as $\pi \rightarrow \pi^*$ type transitions.

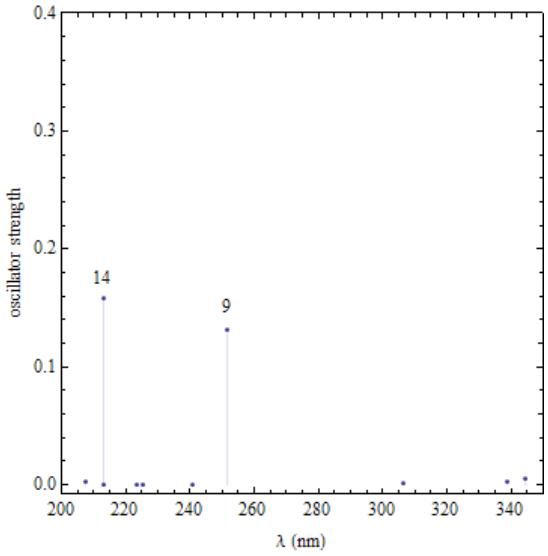

Figure s27. Calculated UV spectrum for pzc ion in water.

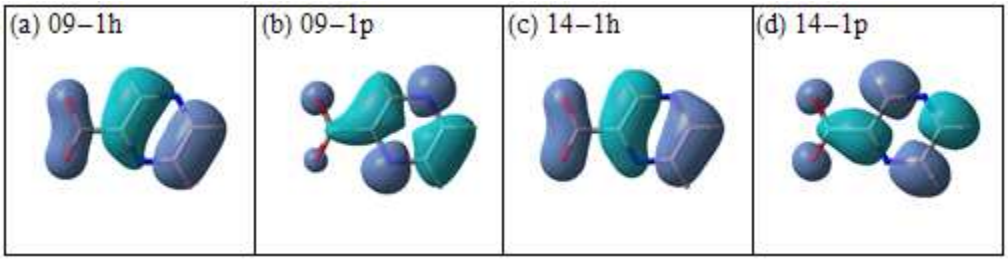

Figure s28. NTO hole/particle pairs for the electronic transitions of pzc ion at 252 and 213 nm.

Compounds **1** and **2**

We have also performed a series of TD-DFT calculations on btc and pzc using molecular geometries taken from the SXRD crystal structure for compounds **1** and **2**. These calculations have been performed for both the bare anions and with the anions in the electrostatic potential field of calcium ions that are represented as static (2+) charges. The simulated spectra for these calculations are compared in **Figure s29**. Panels (a)-(c) show the spectra for the bare btc ion in

compound **1**, the bare btc ion in compound **2**, and the bare pzc ion in compound **2**, respectively. Panels (d)-(f) show the calculated spectra for the three structures but including calcium ions charges. Indeed, the electronic transitions are certainly modified by the presence of the charges, however, the resulting spectra do not seem to correlate with the observed UV DRS spectra for these compounds. Of the three species, the btc ion from compound **1** shows a number of states between 240 and 350 nm that may be connected with the observed absorption bands; however, the calculated oscillator strengths are not in good agreement with the experimental data. We suspect that a more detailed model of the ligand's coordination environment, which explicitly includes the calcium ions and water molecules, is necessary to reproduce the experimental spectrum.

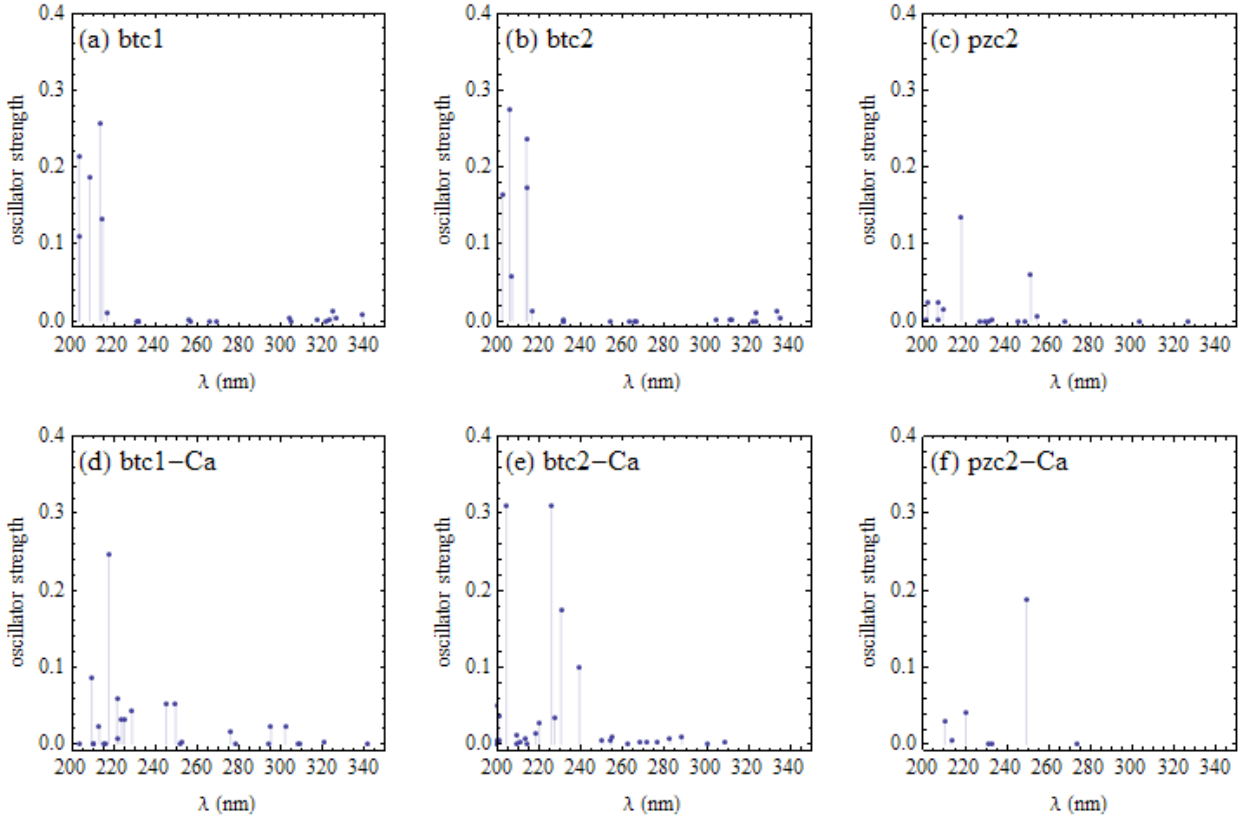

Figure s29. Calculated UV spectra for btc and pzc molecular structures extracted from PXRD data. Panels (a)-(c) do not include calcium ion charges and panels (d)-(f) do include calcium ion charges.